Bulletin of the Seismological Society of America, Vol. , No. , pp. –, , doi: 10.1785/0120190129

Holocene Rupture History of the Central Teton Fault at Leigh Lake, Grand Teton National Park, Wyoming

by Mark S. Zellman, Christopher B. DuRoss, Glenn D. Thackray, Stephen F. Personius, Nadine G. Reitman, Shannon A. Mahan, and Cooper C. Brossy

Abstract Prominent scarps on Pinedale glacial surfaces along the eastern base of the Teton Range confirm latest Pleistocene to Holocene surface-faulting earthquakes on the Teton fault, but the timing of these events is only broadly constrained by a single previous paleoseismic study. We excavated two trenches at the Leigh Lake site near the center of the Teton fault to address open questions about earthquake timing and rupture length. Structural and stratigraphic evidence indicates two surface-faulting earthquakes at the site that postdate deglacial sediments dated by radiocarbon and optically stimulated luminescence to ~10–11 ka. Earthquake LL2 occurred at ~10.0 ka (9.7–10.4 ka; 95% confidence range) and LL1 at ~5.9 ka (4.8–7.1 ka; 95%). LL2 predates an earthquake at ~8 ka identified in the previous paleoseismic investigation at Granite Canyon. LL1 corresponds to the most recent Granite Canyon earthquake at ~4.7–7.9 ka (95% confidence range). Our results are consistent with the previously documented long-elapsed time since the most recent Teton fault rupture and expand the fault's earthquake history into the early Holocene.

Supplemental Material

Introduction

The Teton fault in northwestern Wyoming (Fig. 1) is one of the fastest-moving normal faults in the western United States, accommodating northeast–southwest extension along the northeastern margin of the Basin and Range Province (Puskas *et al.*, 2007; White *et al.*, 2009). The east-dipping fault separates the precipitous eastern margin of the Teton Range in the footwall from the Jackson Hole basin in the hanging wall. The surface expression of the Teton fault extends for ~70 km from its southern end near Wilson to ~5 km north of Jackson Lake (Zellman *et al.*, 2019; Fig. 1) and is characterized by fault scarps formed in glacial, alluvial, and lacustrine landforms and sediments that are late Pleistocene to Holocene. Prominent structural complexities along the Teton fault define three sections, the southern, central, and northern sections (Smith *et al.*, 1993; O'Connell *et al.*, 2003), each about 20–30 km long. The southern and central sections are separated by an ~1-kilometer-wide left step near Phelps Lake; the central and northern sections are defined by an ~2-kilometer-wide right step and fault bend north of Moran Bay (Fig. 1; see Zellman *et al.*, 2019). An open question centers on whether ruptures propagating along the Teton fault are influenced by these structural complexities (Smith *et al.*, 1993; O'Connell *et al.*, 2003). The Teton fault is considered a source of possible large-magnitude earthquakes ($M_w \sim 7$ assuming multisection ruptures) in regional seismic hazard assessments (e.g., Petersen *et al.*, 2014).

Despite the clear postglacial (<14–15 ka; Licciardi and Pierce, 2018; Pierce *et al.*, 2018) geomorphic expression of the Teton fault (Gilbert *et al.*, 1983; Pierce and Good, 1992; Smith *et al.*, 1993; Byrd *et al.*, 1994; Byrd, 1995; O'Connell *et al.*, 2003; Thackray and Staley, 2017), its paleoseismic history remains weakly constrained. For example, the Holocene paleoseismology of the fault is based on observations from only a single trench study—the Granite Canyon site on the southern section (Byrd, 1995; Fig. 1). The Granite Canyon record yields two earthquakes between ~8 and 5 ka, suggesting that the fault has experienced a relatively long period without a surface-faulting earthquake. However, the Granite Canyon study was conducted early in the development of paleoseismic methods and is thus limited by a lack of trench photomosaics, species identification of charcoal samples, luminescence dating, and Bayesian treatment of the geochronological data. Comparison of slip in the Holocene Granite Canyon earthquakes (~3–4 m) with the postglacial slip along the fault suggests that the latest Pleistocene to early Holocene slip rates may exceed Holocene rates by as much as an order of magnitude (Byrd, 1995; White *et al.*, 2009). Thus, our interest in the paleoseismology of the Teton fault is motivated by the early paleoseismic data

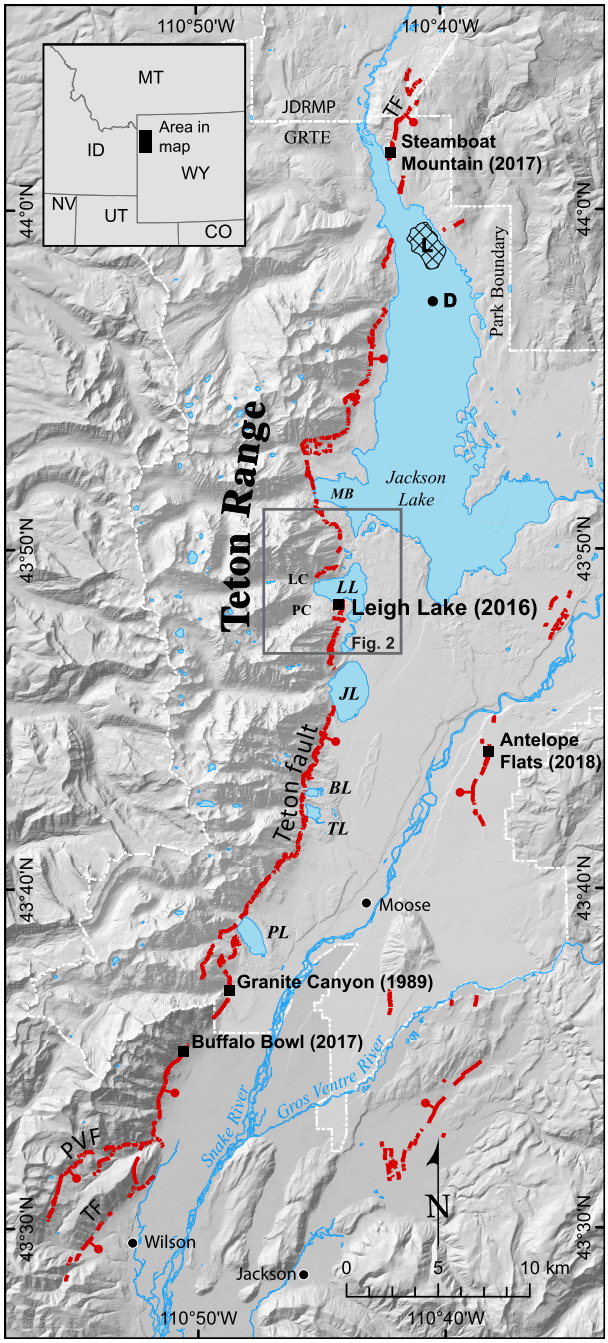

Figure 1. Surface trace of the Teton normal fault (TF) at the base of the Teton Range and other Quaternary faults in Jackson Hole from Zellman *et al.* (2019) shown as bold lines with ball and bar on the downthrown side. Paleoseismic sites shown as squares and labeled with site name; year of trench excavation is included in parentheses. Possible paleoseismic features from Pierce *et al.* (1998) in northern Jackson Lake are labeled "L" (liquefaction) and "D" (backflooded delta). Extents of Grand Teton National Park (GRTE) and John D. Rockefeller Memorial Parkway (JDRMP) are shown. BL, Bradley Lake; CO, Colorado; ID, Idaho; JL, Jenny Lake; LC, Leigh Canyon; LL, Leigh Lake; MB, Moran Bay; MT, Montana; NV, Nevada; PC, Paintbrush Canyon; PL, Phelps Lake; PVF, Phillips Valley fault; TL, Taggart Lake; UT, Utah; WY, Wyoming. See Data and Resources for base map data sources. The inset figure shows the location within northwest Wyoming. The color version of this figure is available only in the electronic edition.

and its compelling impact on the calculation of slip rate, a critical parameter for probabilistic seismic hazard analyses.

To further explore the paleoseismology of the fault, we excavated two trenches at the Leigh Lake site on the central section, about 22 km north of Granite Canyon (Fig. 1). Our primary goals were to define the timing of Holocene surface-faulting earthquakes on the previously unstudied central section of the fault, compare results with the Granite Canyon data for the southern section, and evaluate the completeness of the fault's earthquake record, including whether at least 5 k.y. have elapsed since the most recent surface-faulting earthquake.

Our Leigh Lake paleoseismic study is part of a broader effort to expand our understanding of the timing, recurrence, and displacement of Teton fault earthquakes, and evaluate the rupture lengths of these earthquakes in the context of structural complexities along the fault. Additional paleoseismic investigations include those at Jackson Hole Mountain Resort (Buffalo Bowl site; DuRoss, Gold, *et al.*, 2019), Steamboat Mountain (Zellman *et al.*, 2019), and Antelope Flats (antithetic fault scarp; Thackray *et al.*, 2019; Fig. 1). This article focuses on the Leigh Lake paleoseismic site. We document stratigraphic and structural observations, present geochronological data, and discuss evidence for at least two surface-faulting earthquakes postdating a <15 ka deglacial surface. We present Bayesian models of earthquake timing for the site and compare our results with previous paleoseismic data. Our Leigh Lake study confirms a period of no surface ruptures since ~5 ka and includes a previously unrecorded early Holocene earthquake on the fault at ~10 ka.

Previous Paleoseismic Data

Although Teton fault scarps cut latest Pleistocene deglacial surfaces with about 10.3–13.5 m of vertical separation (VS; Thackray and Staley, 2017), considerable uncertainty remains in the timing of surface-faulting earthquakes on the fault. The Holocene paleoseismology of the southern section of the Teton fault is derived from a single trench excavated across a postglacial alluvial surface at Granite Canyon (Byrd, 1995; Fig. 1). At this site, Byrd (1995) excavated an ~11-meter-long trench across a 3–4-meter-high east-facing fault scarp. Two surface-faulting events postdate a burn horizon formed within alluvial sediments dated to ~8.1 ± 0.2(1σ) ka (all reported ages in Byrd, 1995, were calendar-calibrated here using OxCal; Bronk Ramsey, 2009). The older Granite Canyon earthquake occurred at ~7.8–8.3 ka based on a maximum age from the burn horizon and two minimum ages of 7.9 ± 0.1(1σ) ka and 8.0 ± 0.1(1σ) ka for charcoal sampled from scarp-derived colluvium. The younger Granite Canyon rupture is broadly constrained to between 7.9 ± 0.1 ka and 4.7 ± 0.1(1σ) ka, based on ages for scarp-colluvial deposits predating and postdating the event, respectively.

Liquefaction features and evidence of subsidence of the Snake River delta, both on the hanging wall of the northern section of the Teton fault (Fig. 1), suggest more recent Teton

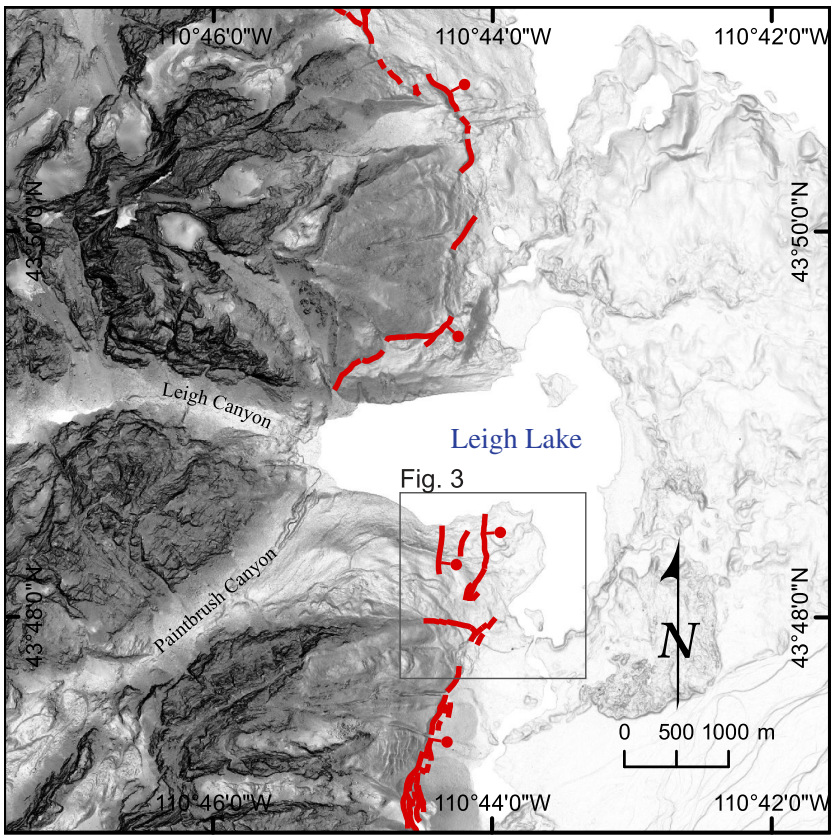

Figure 2. Map showing the Leigh Lake study site in relation to Leigh Lake, Paintbrush Canyon, and Leigh Canyon. The Teton fault from Zellman *et al.* (2019) is shown as bold lines with ball and bar on the downthrown side. Location of Figure 3 is shown. See Data and Resources for base map data sources. The color version of this figure is available only in the electronic edition.

fault earthquakes (Pierce *et al.*, 1998). The features are now submerged beneath northern Jackson Lake but were exposed subaerially in 1987 and 1988 while the lake was temporarily lowered for maintenance at Jackson Lake Dam. The kilometer-scale liquefaction features (arcuate disconnected ridges and filled fractures) suggest intense shaking of a mid-Holocene Snake River delta surface (Pierce *et al.*, 1998). Cultural artifacts that likely postdate the deformation date to ~3–5 ka (Pierce *et al.*, 1998). At the Snake River delta front, paleoshoreline features crosscut deltaic (alluvial) sediments and indicate flooding of the southernmost delta surface, possibly as the result of a >0.7 m subsidence event that occurred prior to ~1.6 ka based on cultural artifacts (Pierce *et al.*, 1998). These features imply strong ground shaking (the liquefaction features) and fault movement (submerged delta front) but are ultimately secondary in nature and thus cannot be uniquely tied to movement of the Teton fault.

The vertical slip rate of the Teton fault remains uncertain because it is constrained only by surface VS measurements and limited paleoseismic data from a single trench. For example, the Holocene slip rate is as low as ~0.2 mm/yr using the Granite Canyon earthquake data (Byrd, 1995) or as high as ~2 mm/yr using the average postglacial VS for the fault of 14 m and subtracting inferred Holocene displacement (Byrd, 1995; White *et al.*, 2009). These differences led Byrd (1995) and White *et al.* (2009) to conclude that the latest Pleistocene to early Holocene slip rate exceeds the Holocene rate for the fault by as much as an order of magnitude. Hampel *et al.* (2007) had a similar result, but they concluded that most slip occurred prior to the Holocene, from 16 to 14 ka. DuRoss, Gold, *et al.* (2019) combined geomorphic and paleoseismic data and showed that the latest Pleistocene to early Holocene slip rate only exceeds the Holocene rate by a factor of ~2. The postglacial to present slip rate is ~0.8 mm/yr using a revised estimate of ~11 m of VS across deglacial surfaces formed at ~14–15 ka (Thackray and Staley, 2017; Licciardi and Pierce, 2018; Pierce *et al.*, 2018).

Leigh Lake Study Site

At the Leigh Lake site on the central section of the Teton fault, scarps are formed on a deglacial surface adjacent to Leigh Lake at the outlets of Paintbrush and Leigh Canyons (Fig. 2). The Leigh Lake deglacial surface (Fig. 3a) and landforms (e.g., moraines and kettles; Fig. 3b) were formed during the latest phase of the Pinedale glaciation (Jackson Lake phase, or phase Pd-3 ending at ~14–15 ka; Licciardi and Pierce, 2018; Pierce *et al.*, 2018). During this glacial period, mountain-valley glaciers sourced from the Teton Range advanced east over the site and into Jackson Hole where they met southward-advancing ice lobes sourced from the Greater Yellowstone Glacial System (Pierce *et al.*, 2018).

Postglacial movement of the Teton fault at the Leigh Lake site is expressed as three subparallel east-facing fault scarps (Fig. 3b). These scarps, herein the western, central, and eastern scarps, have ~1.2–2.9 m, ~1.1–2.3 m, and ~1.4–2.0 m of VS, respectively (see the Ⓔ supplemental material to this article). These scarps yield a VS sum of ≤7.2 m, in contrast to an average VS of 11.1 m for deglacial surfaces measured at Taggart Lake, Bradley Lake, and Granite Canyon (Thackray and Staley, 2017; Fig. 1). The apparent decrease in postglacial displacement at Leigh Lake may be related to an ~1.5 km left step in the trace of the Teton fault at Leigh Lake (Fig. 2). In this area, the trace of the fault splinters into multiple normal and apparent oblique-slip fault scarps (Fig. 3b). We suspect that unidentified deformation associated with this structural complexity indicates that our total VS measurement is a minimum value.

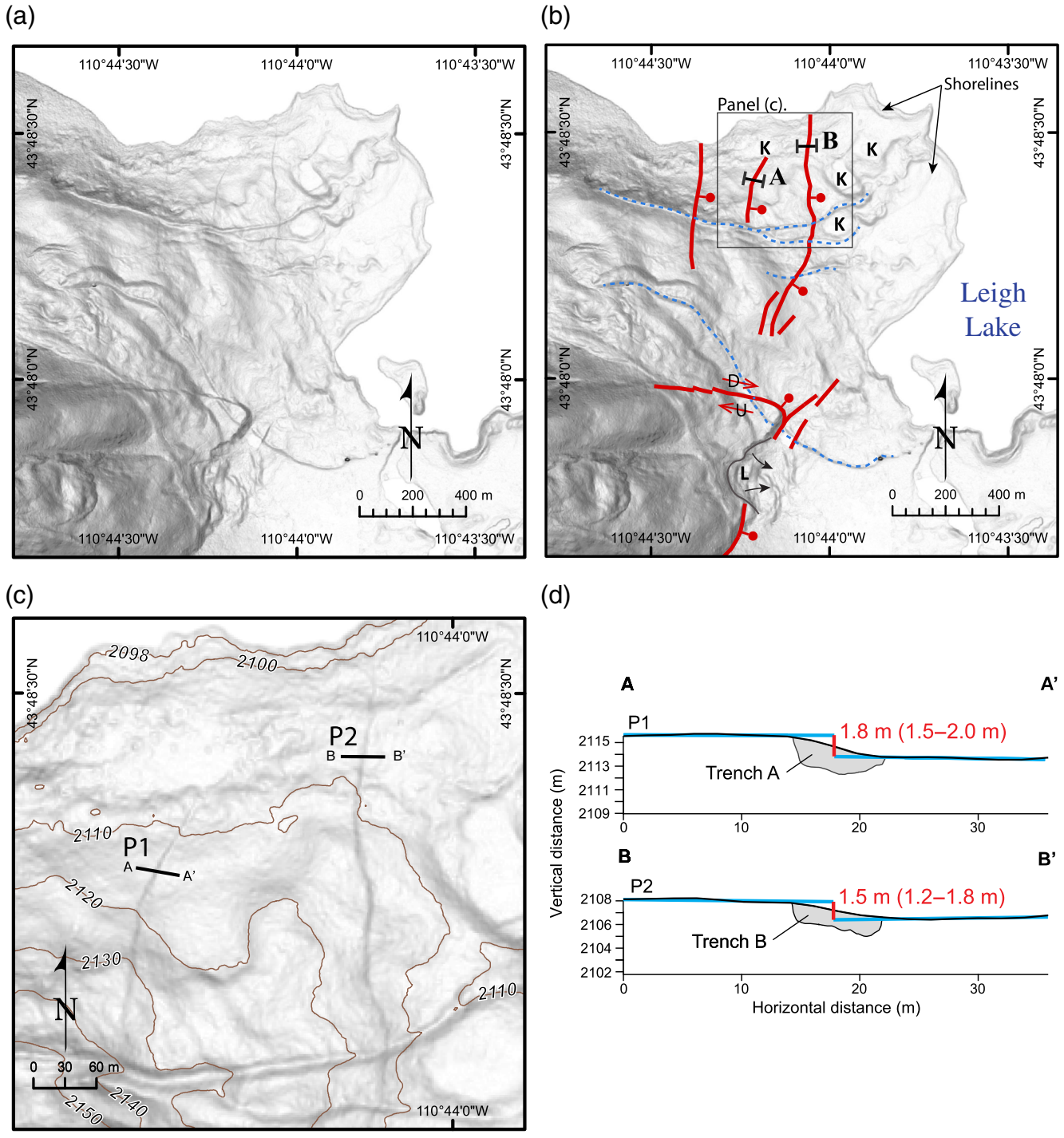

Figure 3. (a) Uninterpreted and (b) interpreted light detection and ranging (lidar) slope map (steeper slopes shown as darker shades of gray) images of the Leigh Lake site. In (b), trenches (black bars) include "A" across the central scarp and "B" across the western scarp. Scarps related to the Teton fault are shown as bold with the ball and bar on downthrown side. Arrows indicate inferred lateral motion. Dashed lines are moraine crests, and kettles are labeled with "K." Shorelines are labeled. A landslide is labeled "L" and arrows show direction of slope movement. (c) Detailed view shows location of topographic profiles P1 (trench A) and P2 (trench B), 2 m contours are shown and labeled, and black arrows point to fault scarps. (d) Topographic profiles P1 and P2 are shown with trench outlines and vertical separation (VS) across scarp calculated using multiple profile iterations (Ⓔ Table S3, available in the supplemental material to this article) after DuRoss, Bunds, *et al.* (2019). Preferred VS is labeled with minimum and maximum shown in parentheses. Lidar data from GRTE (see Data and Resources). The color version of this figure is available only in the electronic edition.

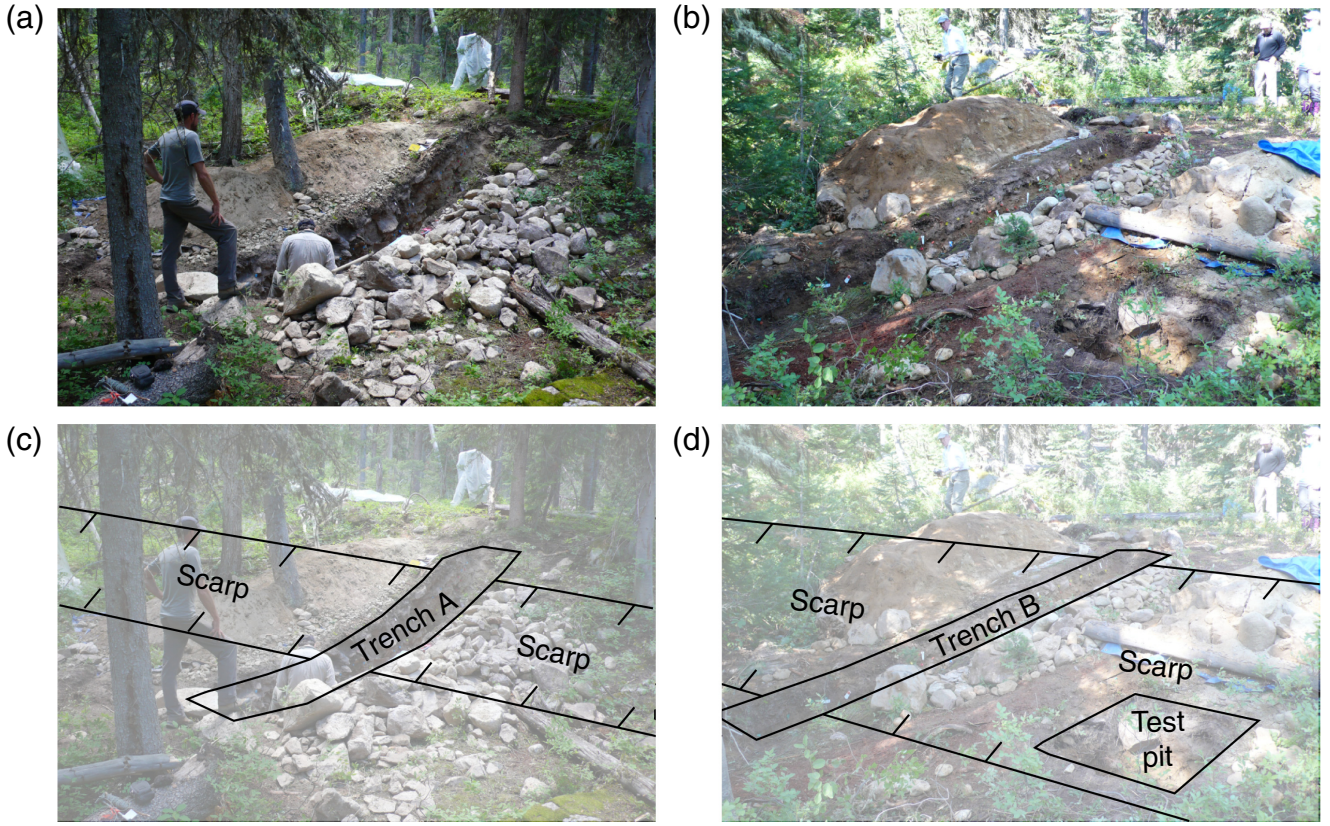

Figure 4. Photographs of Leigh Lake trench sites (a) A and (b) B; (c, d) the trench (and test pit) locations in the context of the Teton fault scarp. View is to the southwest. Photos by M. Zellman. The color version of this figure is available only in the electronic edition.

Methods

We excavated trenches across the central (trench A) and eastern (trench B) Leigh Lake fault scarps (Fig. 3). The Leigh Lake site allowed us to investigate the timing of earthquakes on the central section of the Teton fault, where there are no previous paleoseismic data. Further, moderate (~1–3-meter-high) fault scarps permitted excavation with hand tools, as opposed to the larger late Pleistocene scarps found elsewhere along the fault.

Trenches A and B (Fig. 4) crossed the central and eastern fault scarps (Fig. 3b). Trench A traversed the central scarp at an orientation of 100° (Figs. 3b and 4) and measured ~7 m long, ~1 m wide, and ≤1.5 m deep. Trench B crossed the eastern scarp at an orientation of 90° (Figs. 3b and 4) and was ~6 m long, ~1 m wide, and ≤1 m deep. We excavated a test pit (1 m × 1 m × 1 m) adjacent to trench B to provide an additional exposure of stratigraphic contacts at the eastern end of the trench. The pit was located ~3 m north of the eastern end of trench B (Fig. 4d). We did not investigate the western scarp because of its more subtle geomorphic expression, larger displacement, and difficult access.

To record the trench exposures, we created photomosaics (following the methods of Reitman *et al.*, 2015). The photomosaics as well as stratigraphic and structural relations and geochronological data are shown in Figures 5a,b (Trench A) and 6a,b (Trench B). Stratigraphic units are described in Ⓔ Tables S1 and S2.

We used optically stimulated luminescence (OSL) and radiocarbon (^{14}C) dating to constrain the depositional ages of stratigraphic units exposed in the trenches (Tables 1 and 2). OSL samples were collected following protocols outlined by Gray *et al.* (2015) and consisted of quartz grains from fine sand sampled from the stratigraphic units. These OSL ages represent the time since grain transport and daylight exposure prior to deposition and burial (Rhodes, 2011; Gray *et al.*, 2015). Radiocarbon samples consisted of macro charcoal fragments from the stratigraphic or pedogenic units as well as those separated from bulk organic sediment. Charcoal identification, in some cases to the genus or species level (Table 2), allowed us to identify and date the shortest-lived samples local to the site. The ^{14}C ages generally represent the age of soil formation within the sampled stratigraphic unit. We used OxCal (Bronk Ramsey, 2009) to calendar-calibrate the ^{14}C ages. A total of eight ^{14}C ages (Table 2) and nine OSL ages (Table 1) constrain the timing of unit deposition and soil horizon formation at Leigh Lake (Figs. 5 and 6).

Earthquake timing was evaluated with OxCal Bayesian modeling software (v.4.3; Bronk Ramsey, 2009). We include both Leigh Lake trenches in two OxCal models (Fig. 7; Ⓔ OxCal Code S1) using stratigraphic ordering included

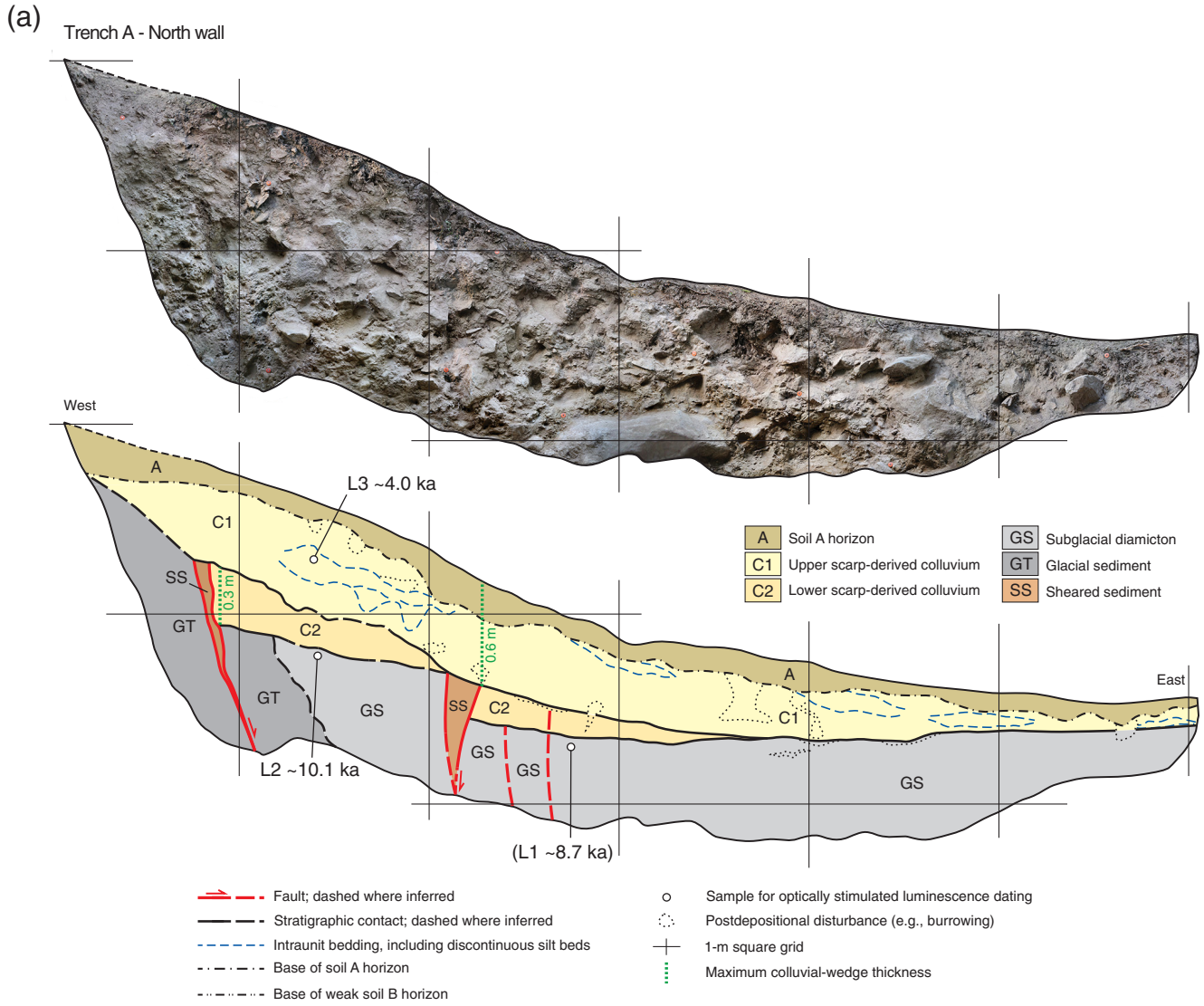

Figure 5. Stratigraphic and structural relations in (a) the north and (b) south walls of trench A. The south wall of trench A is shown as a mirror image. Uninterpreted photomosaics were constructed using the methods of Reitman *et al.* (2015). Stratigraphic units are described in the Stratigraphic Units and Fault Structure section and Ⓔ Table S1. Mean ages are shown for optically stimulated luminescence (OSL) and charcoal radiocarbon (^{14}C) samples (Tables 1 and 2, respectively). Ages excluded from Bayesian models are shown in parentheses; a toggled age is shown in brackets. Vertical and horizontal grid lines are 1 m apart. Vertical dotted lines show maximum colluvial wedge thicknesses, which we interpret as per-event displacement minima. (*Continued*)

in a prior model, ^{14}C and OSL ages and uncertainties, and a historical constraint of no large surface-faulting earthquakes of the Teton fault since Jackson Hole settlement in 1884 (Fig. 8).

Results

Stratigraphic Units and Fault Structure

Trench A (central scarp) and trench B (eastern scarp) exposed clastic sediments related to Pinedale glaciation of the region and faulting from at least two Teton fault earthquakes. In both trenches, sedimentary packages include (1) massive poorly sorted greenish sand and gravel with cobbles and boulders that we interpret as subglacial diamicton or till (unit GT), (2) massive poorly sorted brown silt, sand, and gravel with cobbles and boulders that we interpret as late-stage glacial (likely outwash) sediment (unit GS), and (3) massive loose poorly sorted sand and gravel with local accumulations of silt and organic matter that we interpret as scarp-derived colluvium eroded from the footwall following surface faulting along the Teton fault (units C, C1, and C2; see also the Ⓔ supplemental material). Evidence in support of a tectonic interpretation for the colluvial units is included later. Although units GT and GS have minor textural differences between the trench exposures (e.g., clast angularity and sorting), the close proximity of the trenches, common depositional setting, and sediment ages suggest that these

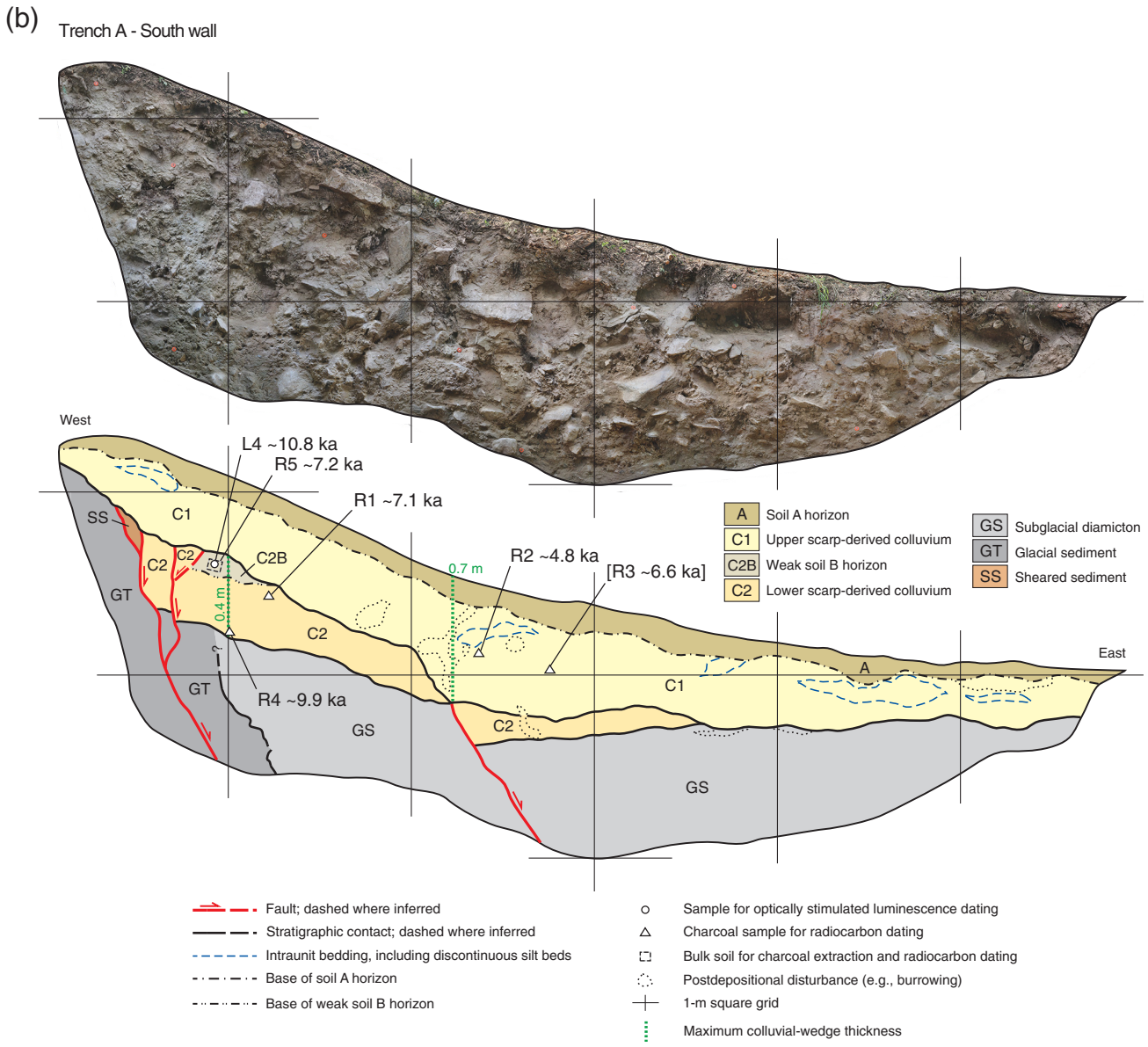

Figure 5. Continued.

differences are due to lateral heterogeneity within the units. We used sediment texture (clast sorting and slope-parallel fabric), structure (e.g., upward fault terminations), and pedogenic units within the deglacial and colluvial sediments to differentiate between the colluvial units and deglacial deposits.

Stratigraphic units in trench A include glacial units GT and GS, which are overlain by two scarp-derived colluvial units: C2 (lower) and C1 (upper) (Fig. 5a,b). We differentiated between C2 and C1 using sediment texture, the presence of discontinuous silt beds restricted to unit C1, upward fault terminations at the C2–C1 contact, and a weak soil B horizon formed within the uppermost part of unit C2 (unit C2B). Soil unit C2B is characterized by an accumulation of silt and blocky soil structure. Units C2 and C1 are a maximum of 0.6–0.7 m and 0.3–0.4 m thick, respectively (Fig. 5a,b). Although a steeply east-dipping contact between GT and GS occurs near the fault zone exposed in trench A, we interpreted this contact as depositional as it has a wavy geometry and lacks any evidence of shear fabric (e.g., rotated clasts) along it. A soil A horizon is formed at the surface in the uppermost part of unit C1.

The Teton fault is expressed as a relatively simple fault zone in trench A (Fig. 5a,b). Two primary down-to-the-east faults locally consist of ~5-centimeter-wide zones of shearing. These faults dip ~60°–90° E, and vertically displace units GT, GS, and C2. Both faults terminate upward at the base of unit C1. Trench A did not fully expose the planar uneroded top of units GT/GS in the footwall, and thus, we are unable to measure the vertical displacement of these units.

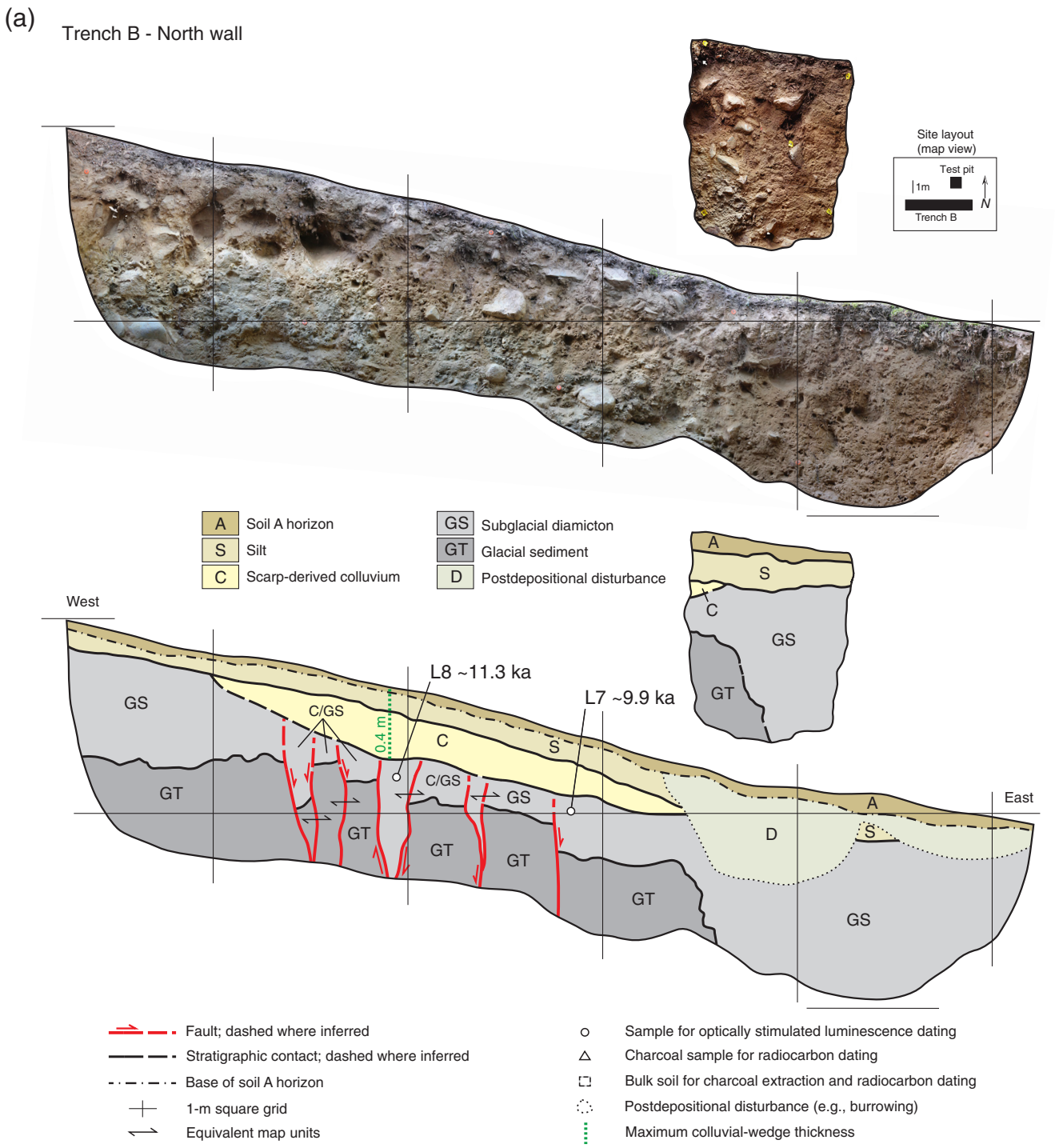

Figure 6. Stratigraphic and structural relations in (a) the north and (b) south walls of trench B. The south wall of trench B is shown as a mirror image. Uninterpreted photomosaics were constructed using the methods of Reitman *et al.* (2015). (a) The trench B north-wall panel includes an ~1-meter-deep test pit excavated ~1 m north of the trench. Similar to trench B, the test pit did not expose evidence of faulting at the unit GS–GT contact. Stratigraphic units are described in the Stratigraphic Units and Fault Structure section and Ⓔ Table S2. Mean ages are shown for OSL and charcoal radiocarbon (^{14}C) samples (Tables 1 and 2, respectively). An age excluded from Bayesian models is shown in parentheses. Vertical and horizontal grid lines are 1 m apart. Vertical dotted lines show maximum colluvial wedge thicknesses, which we interpret as per-event displacement minima. (*Continued*)

Trench B exposed units GT and GS but only a single scarp-derived colluvial unit, unit C (Fig. 6a,b). Unit C is overlain by a silt-rich deposit (unit S), a well-developed A horizon at the ground surface (unit A), and zones of biological disturbance (unit D). Unit C is a maximum of about 0.4 m thick and overlies units GT and GS, as well as sediment-filled fissures

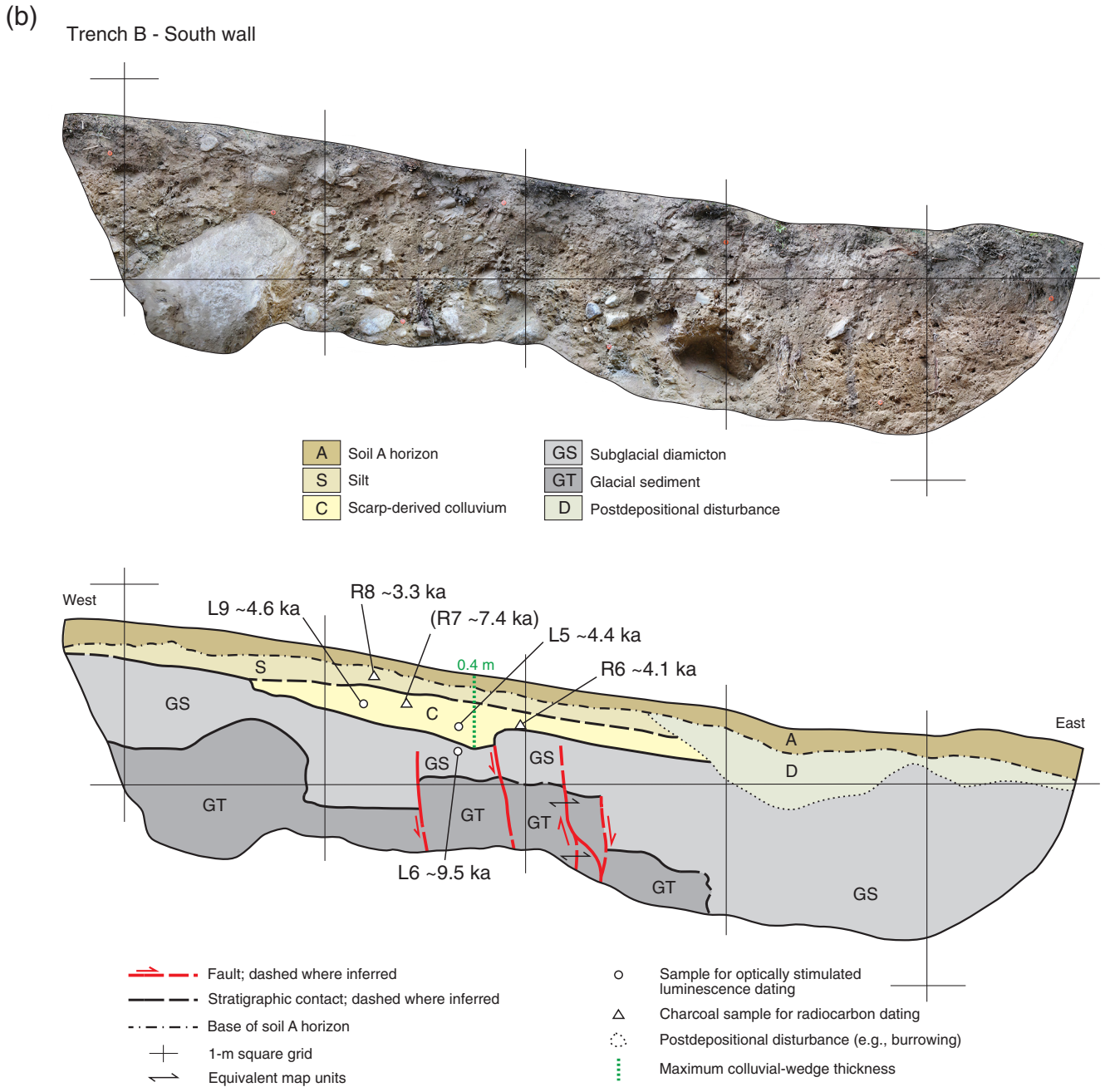

Figure 6. Continued.

forming unit C/GS (Fig. 6a,b). In trench B, unit GS appears to conformably overlie (western to central part of trench) to unconformably overlie (eastern end) unit GT. Near the eastern end of the trench, unit GS thickens along a near-vertical irregular contact with basal unit GT (Fig. 6a,b). This stratigraphic relationship is expressed in both walls at the same location in the trench, but it is best expressed in the north wall because boulders obscure a clear exposure of the contact on the south wall. The test pit, ~3 m north of trench B, duplicated this exposure and stratigraphic relationship (Fig. 6b). We interpret the steep GT–GS contact to be depositional because of its irregular geometry and the lack of evidence of faulting or shearing in any of the exposures (Fig. 6b).

The Teton fault is expressed as a distributed, ~2-meter-wide fault zone in trench B (Fig. 6a,b). The faults are steeply dipping (75°–90°) and best expressed on the north wall where they bound narrow (decimeter-scale) grabens. Faults in trench B displace unit GT down-to-the east about 0.5 m and terminate upward against the base of unit C or become indistinguishable within unit GS.

Table 1
Optically Stimulated Luminescence (OSL) Ages for the Leigh Lake Trench Site

Sample Number*	Unit†	Age—Mean ± 1σ (yr B.P.)‡	Water Content§	*K* (%)‖	U (ppm)‖	Th (ppm)‖	Total Dose Rate (Gy/ka)#	Equivalent Dose (Gy)**	*N*††	Scatter (%)‡‡
L1[E]	GS	8,670 ± 550	4 (28)	2.34 ± 0.11	6.84 ± 0.44	10.4 ± 0.60	4.60 ± 0.16	40 ± 2.1	2 (15)	68
L2	GS	10,070 ± 1,050	4 (23)	2.14 ± 0.09	5.50 ± 0.32	7.97 ± 0.63	4.04 ± 0.16	41 ± 3.9	3 (24)	76
L3	C1	4,000 ± 510	3 (25)	2.26 ± 0.04	5.39 ± 0.25	9.28 ± 0.41	4.23 ± 0.11	17 ± 2.1	3 (15)	102
L4	C2B	10,840 ± 1,020	3 (24)	1.87 ± 0.08	3.67 ± 0.26	10.7 ± 0.72	3.57 ± 0.15	39 ± 3.2	2 (15)	71
L5	C2	4,430 ± 630	6 (29)	1.99 ± 0.03	5.02 ± 0.17	13.1 ± 0.24	4.13 ± 0.05	18.3 ± 2.6	5 (24)	43
L6	GS	9,525 ± 805	6 (30)	1.85 ± 0.09	4.81 ± 0.33	11.0 ± 0.78	3.77 ± 0.17	35.9 ± 2.6	2 (24)	55
L7	GS	9,930 ± 510	5 (21)	2.27 ± 0.05	4.97 ± 0.31	11.1 ± 0.53	4.32 ± 0.13	42.9 ± 1.8	6 (24)	32
L8	C/GS	11,300 ± 955	6 (28)	1.93 ± 0.11	5.46 ± 0.40	11.0 ± 0.98	4.00 ± 0.21	45.2 ± 3.1	1 (15)	40
L9	C	4,650 ± 345	7 (31)	1.54 ± 0.05	4.07 ± 0.37	8.09 ± 0.56	3.16 ± 0.10	14.7 ± 1.0	3 (20)	51

*Samples processed by the U.S. Geological Survey Luminescence Dating Laboratory (Denver, Colorado). Superscript "E" indicates sample excluded from OxCal Bayesian models, see the Geochronology section for discussion..

†Stratigraphic unit sampled (Fig. 3; Ⓔ Tables S1 and S2, available in the supplemental material to this article).

‡Mean and 1σ OSL age before sample processing date (2014), using exponential fit on equivalent doses; ages and errors rounded.

§Field moisture percentage based on weight; complete sample saturation percent in parentheses. Ages calculated using ~20% of the saturated moisture.

‖Background radiation for bulk sediment from the sample location; analyses obtained using high-resolution gamma spectrometry (high-purity germanium [Ge] detector).

#Total dose includes cosmic doses (~0.28–0.23 Gy/ka) and attenuation with depth calculated using the methods of Prescott and Hutton (1994). Gy, gray.

**Equivalent dose (D_e) calculated using the number of replicated D_e estimates.

††Number (N) of replicated D_e estimates used to calculate the final overall D_e. Numbers in parentheses indicate total number of measurements included in calculating the represented D_e and age using either the minimum age model for dispersions >25% or the central age model for dispersions <25%.

‡‡Defined as overdispersion of the D_e values and obtained by the "R" radial plot program. Values >30% are considered to be poorly bleached or mixed sediments.

Evidence of Surface-Faulting Earthquakes

In trench A, unit C1 has abundant structural, geometric, and pedogenic evidence in support of a surface-faulting earthquake origin. The basal contact of unit C1 is the upward termination point for several faults that displace units GT, GS, and C2 (Fig. 5a,b). Unit C1 has a wedge-shaped geometry, which is the thickest (~0.6–0.7 m) at the base of the fault scarp, and unconformably overlies faulted soil C2B and faulted and back-rotated unit C2. Soil unit C2B, the youngest faulted deposit at the site, forms a paleosurface that separates scarp-colluvial units C2 and C1, and suggests surface stability (soil development) prior to rupture.

Unit C2 (trench A) has moderate evidence in support of an earthquake origin. Unit C2 is vertically displaced by faults activated in the youngest earthquake at the site. The unit is not as thick or laterally extensive as unit C1, but it has a wedge-shaped geometry (thinning to the east) and unconformably overlies the near-vertical stratigraphic contact between units GT and GS. A subsidiary fault in unit GS may predate C2 deposition (terminating upward at the basal C2 contact; Fig. 5b); however, evidence in support of this is weak because of the coarse nature of units GT/GS and C2. Although C2 is textually similar to units GT/GS, it is looser with dispersed organics, a characteristic that sets it apart from the inorganic glacially derived units. Because we only have moderate structural evidence in support of C2 (one possible upward fault termination), we cannot fully rule out a gravitational or storm-related origin for the unit. However, considering the gentle nearly horizontal surface geomorphology at the site (Fig. 3d), we consider a tectonic origin for unit C2 to be most likely. That is, prior to surface faulting, only subtle relief existed at the site. Thus, colluvial sedimentation in unit C2 is likely evidence of scarp formation and exposure of units GT and GS, degradation of the scarp, and colluvial deposition on the hanging wall of the fault.

In trench B, unit C has primarily structural and stratigraphic evidence in support of an earthquake origin. Unit C unconformably overlies a distributed zone of faulting and fissure formation within units GS and GT (Fig. 6a,b). Individually, these faults have centimeter scale down to the east and west motion (net displacement is east down) and terminate upward at the basal unit C contact. Fissures formed in units GT and GS, filled with inorganic sediment (unit C/GS; Fig. 6a), and buried by unit C provide additional evidence for surface faulting at the site. Unit C as well as an overlying silt deposit (unit S) reaches a maximum thickness of ~0.4 m where they overlie this zone of deformation. Unit C has an approximate wedge shape, thinning toward the scarp crest and base. Similar to trench A, we did not find evidence of a pedogenic horizon on the glacially derived units where buried by scarp colluvium.

Weak evidence suggests the possibility of an older surface rupture related to unit C/GS in trench B. Unit C/GS consists of inorganic sand-rich colluvial sediment likely derived from unit GS and restricted to fissures formed in a distributed fault zone (Fig. 6a). It is possible that unit C/GS is related to minor (centimeter-scale) surface rupture at the site, and thus represents an older deposit of scarp colluvium. However, because of a lack of soil formation within unit C/GS, differential displacements with depth, or an older package of scarp-derived colluvium similar in geometry and texture to unit C, we prefer a simple explanation that fissure formation is contemporaneous with scarp colluvial unit C.

Table 2
Radiocarbon Ages for the Leigh Lake Trench Site

Sample Number*	Unit†	Calibrated Age—Mean ± 1σ (yr B.P.)‡	Location§	Sample Description‖	Lab Age (^{14}C yr B.P.)#	Delta C-13**	CAMS Number††	Accession Number‡‡
R1	C2	7108 ± 63	A, N wall	Rosaceae charcoal (8.4 mg)	6.84 ± 0.44	−25	176699	
R2	C1	4750 ± 76	A, N wall	Rosaceae charcoal (8.4 mg)	5.50 ± 0.32	−25	176700	
R3^{T}	C1	6558 ± 51	A, N wall	Parenchymous tissue (8.1 mg)	5.39 ± 0.25	−25	176701	
R4	C2	9886 ± 119	A, N wall	Pseudotsuga menziesii (13.3 mg)	3.67 ± 0.26	−23.04		OS-134327
R5	C2B	7222 ± 36	A, N wall	Unidentified hardwood twig charcoal (6.0 mg)	5.02 ± 0.17	−25	176702	
R6	C	4066 ± 60	B, S wall	Populus charcoal (54.2 mg)	4.81 ± 0.33	−25	176703	
R7^{E}	C	7376 ± 35	B, S wall	Pinus (hard) (20.2 mg)	4.97 ± 0.31	−25.21		OS-134328
R8	S	3316 ± 39	B, S wall	Rosaceae charcoal (5.6 mg)	5.46 ± 0.40	−25	176704	

*Samples processed by the National Ocean Sciences Accelerator Mass Spectrometry (NOSAMS) facility, Woods Hole Oceanographic Institution (Woods Hole, Massachusetts). Superscript "E" indicates sample excluded from OxCal Bayesian models; superscript "T" indicates sample "toggled" between OxCal Bayesian models (i.e., excluded from OxCal model 1 (preferred) and included in OxCal model 2 (alternate); see the Geochronology section for discussion.
†Stratigraphic unit sampled (Fig. 3; Ⓔ Tables S1 and S2).
‡Calendar-calibrated age before A.D. 1950 (cal B.P.). Calendar calibrated using OxCal (v.4.3; Bronk Ramsey, 2009). Ages and errors rounded to nearest decade.
§Trench (A or B) and wall (south [S] or north [S]) where sample was collected.
‖Charcoal separation and identification by PaleoResearch Institute (Golden, Colorado). Sample weight (mg) in parentheses. UID, unidentified charcoal.
#Laboratory-reported radiocarbon age is mean and 1σ uncertainty in ^{14}C yr B.P.
**Measured delta ^{13}C.
††Samples processed by Center for Accelerator Mass Spectrometry (CAMS), Lawrence Livermore National Lab (Livermore, California).
‡‡Samples processed by the NOSAMS facility, Woods Hole Oceanographic Institution (Woods Hole, Massachusetts).

Geochronology

The timing of unit deposition and soil horizon formation at Leigh Lake is constrained by eight ^{14}C ages (Table 2) and nine OSL ages (Table 1). These ages are in general stratigraphic agreement and provide limits on the timing of surface faulting at the site. However, we exclude one OSL age (L1) and one ^{14}C age (R7) on account of stratigraphically inconsistent ages possibly resulting from post depositional erosion and recycling and/or biological mixing of sediment (discussed later). These two samples are excluded from further analysis. We included the remaining seven ^{14}C ages (Table 2) and eight OSL ages (Table 1) in our OxCal time-stratigraphic Bayesian models.

In trench A, eight of nine ages constrain the depositional ages of units GS, C1, and C2. OSL sample L2 yields an age for the uppermost part of unit GS of ~10.1 ka. We exclude an additional age for uppermost unit GS of ~8.7 ka (L1) from our Bayesian modeling. L1 is inconsistent with (~1.4 ka younger than) L2 and may have sampled the basal part of unit C2. Two ^{14}C ages constrain the deposition of unit C2 to between ~9.9 ka (R4; basal part of unit) and ~7.1 ka (R1; upper part of unit). Although R4 (~9.9 ka) is close to the age of unit GS (~10.1 ka) and because of its sample position at the base of the C2 colluvial wedge, it could represent material eroded from the fault scarp free face. However, we include the age in our OxCal model because units GT and GS are barren and thus unlikely to be a source of charcoal eroded from the fault scarp and deposited in the colluvial wedge. Further, the lack of soil development on GS/GT, where buried by C2 suggests that these glacially derived units did not have a soil A horizon present within them at the time of surface faulting and deposition of unit C2. We consider it more likely that R4 represents charred plant matter incorporated into unit C2 during the early Holocene, after surface faulting. Soil development (unit C2B) within the uppermost part of unit C2 occurred at ~7.2 ka (R5) and possibly as early as ~10.8 ka (L4). The 10.8 ka age for L4 appears to conflict with the ~10.1 ka age (L2) for unit GS stratigraphically below it; however, we include L4 in our Bayesian models because of its broad uncertainty, ~3 ka of temporal overlap with L2, and similarity to R4 (~9.9 ka), also sampled from unit C2. Scarp colluvial unit C1 was deposited at ~4.0–4.8 ka (L3, R2), and possibly as early as ~6.6 ka (R3). Although R3 is stratigraphically consistent with R1 and R5 (~7.1–7.2 ka) for C2/C2B, we exclude the age from our preferred Bayesian model as uncertainty in the context of the sample remains. (Could material recycled from unit C2 or soil horizon C2B in the fault footwall have been sampled?) Including this age forces the timing of rupture at the site to a narrow (~6.5–7.1 ka) time range (discussed later).

In trench B, seven of eight ages constrain the depositional ages of units GS, C, and S. The uppermost part of unit GS is constrained to ~9.5–11.3 ka based on three consistent OSL ages (L6, L7, and L8). One ^{14}C (R6) and two OSL (L5 and L9) ages constrain the deposition of unit C to between ~4.1 and ~4.7 ka. An additional ^{14}C age (R7) suggests earlier unit C deposition at ~7.4 ka; however, this age is several thousand years older than R5, R6, and R9. Although R7 is stratigraphically consistent with unit GS, we exclude the age from our Bayesian analysis as we do not have sufficient confidence in its context to use it as a minimum estimate of rupture timing. Unit S overlies unit C and is constrained to ~3.3 ka by a single ^{14}C age (R8).

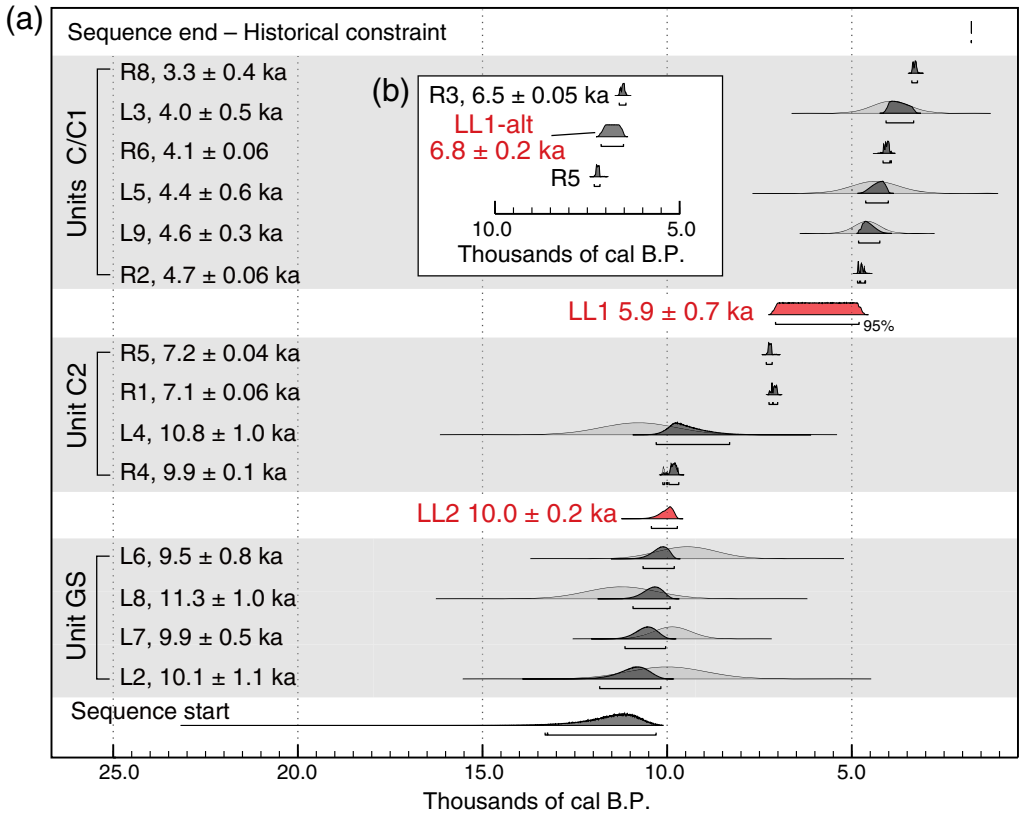

Figure 7. OxCal Bayesian models for the Leigh Lake site showing the probability density functions (PDFs) for ^{14}C and OSL ages that constrain timing for earthquakes LL1 and LL2. (a) Model 1 (preferred) excludes ^{14}C age R3 and yields a broad age range for LL1. (b) An alternate model (model 2) that includes age R3 and yields a tightly constrained age for LL1 (LL1-alt). OSL age L1 and ^{14}C age R7 are excluded from both Bayesian models (see the Bayesian Modeling section for discussion). The color version of this figure is available only in the electronic edition.

Bayesian Modeling

Using our stratigraphic and structural observations from trenches A and B, we develop a simple prior (stratigraphic) model for the Leigh Lake site (Fig. 7). Glacial unit GT and overlying unit GS form the oldest units at the site. These units are faulted and overlain by scarp-colluvial unit C2 (trench A). Unit C2 is faulted and overlain by unit C1 in trench A. We also infer that unit C in trench B is stratigraphically correlative with unit C1. These units have very similar stratigraphic and textural properties—they consist of massive loose poorly sorted silt-rich deposits of colluvium that postdate most recent faulting at the site. Weak evidence of older scarp colluvium in trench B (unit C/GS) and similar geochronological results also support a correlation between units C1 and C. Unit C predates the silt-rich deposit (unit S) exposed in trench B.

We used our geochronological results to construct two OxCal Bayesian models for the site (Fig. 7). Model 1 applies six ^{14}C and eight OSL ages from trenches A and B to our Leigh Lake prior model. An alternative model (model 2) includes not only the same 14 ages but also the age for ^{14}C sample R3, which constrains the deposition of unit C1 in trench A to a minimum of ~6.6 ka. Because R3 exerts significant control on the timing of the youngest earthquake at the site, we toggle it on and off in separate models. Model 1 excludes the R3 minimum age, whereas model 2 includes it. Both models are viable; however, we prefer model 1 (excluding R3) as it yields a broader more conservative earthquake time range and is most consistent with the six ages for C1 (L3, L5, L9, R2, R6, R8; Tables 1 and 2) that are <5 ka (Fig. 7). The tightly constrained age of LL1-alt in model 2 may be valid; however, it is possible that R3, which controls the LL1-alt minimum age, could represent the age of colluvial material recycled from the footwall. Because we consider the narrow LL1 time from model 2 to be less defensible than the broader result from model 1, we do not combine these OxCal model results to yield a single composite earthquake probability density function (PDF) (e.g., DuRoss *et al.*, 2018).

Earthquake Timing and Displacement

OxCal models 1 and 2 indicate that two earthquakes ruptured the Leigh Lake site between ~10.0 (earthquake LL2) and ~5.9 ka (earthquake LL1) (Table 3). In both models, LL2 has an earthquake-timing PDF that yields a mean time of 10.0 ka and a 95% confidence range of 9.7–10.4 ka

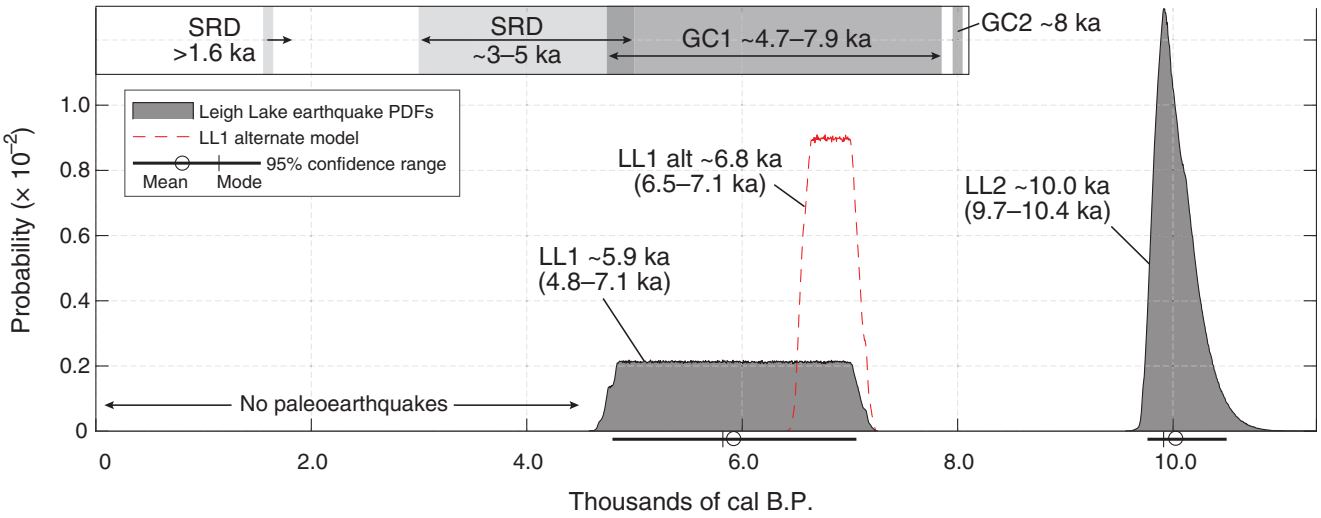

Figure 8. Summary of earthquake-timing data for the Leigh Lake site. Earthquake PDFs generated using OxCal Bayesian modeling software (Bronk Ramsey, 2009; Fig. 7). Alternate model (LL1-alt; Fig. 7) results for LL1 timing shown with a dashed line. Inset area shows previous paleoseismic data, including Granite Canyon earthquakes GC2 and GC1 based on ^{14}C ages in Byrd (1995) and liquefaction and subsidence events inferred along the Snake River delta (SRD) from Pierce *et al.* (1998). The color version of this figure is available only in the electronic edition.

(Fig. 8). The models yield differing but overlapping age ranges for LL1. In model 1, the LL1 PDF (Fig. 8) has a mean time of ~5.9 ka and a 95% confidence range of 4.8–7.1 ka. Model 2, which includes the 6.6 ka minimum age, LL1 (labeled "LL1 alt" in Fig. 8) is constrained to a mean of ~6.8 ka and has a 95% confidence range of 6.5–7.1 ka. As earlier, we prefer the broader LL1 time range, which does not rely on the single age suggesting an older earthquake time before ~6.6 ka.

The vertical displacements for LL1 and LL2 are poorly constrained because of the limited lengths of the trenches and, thus, exposures of the deglacial sediments outside of the zone of faulting. Summing the maximum thickness of the scarp-colluvial units (C1 and C in trenches A and B, respectively) suggests minimum displacements of 1.1 m for LL1 and 0.4 m for LL2 (Figs. 5 and 6). In contrast, VS values for the Leigh Lake deglacial surface (Fig. 3) suggests that LL1 and LL2 had a total of ~3.3 m of displacement (see the Ⓔ supplemental material). Using the minimum colluvial thicknesses and dividing the 3.3 m VS equally between the events, we estimate vertical displacements of ~1.1–1.7 m for LL1 and ~0.4–1.7 for LL2 (Table 3). However, these are likely minimum displacements as it is unknown whether earthquakes LL1 and LL2 also ruptured the western scarp.

Discussion

Paleoseismology of the Leigh Lake site

Trenches excavated across two of three scarps at the Leigh Lake site (Fig. 3) yield a record of two Holocene surface-faulting earthquakes. Earthquake LL2 occurred at ~10.0 ka (9.7–10.4 ka; 95% confidence range), had ~0.4–1.7 m of vertical displacement, and is only expressed in the central scarp. However, we cannot rule out the possibility that LL2 also ruptured the eastern scarp and

Table 3
Earthquake Timing and Recurrence at the Leigh Lake Site

	Earthquake Timing† (cal B.P.)				
Earthquake*	Mean	1σ	50%	95%	Displacement‡ (m)
LL2	10,030	190	10,000	9,720–10,430	0.4–1.7
LL1	5,930	680	5,930	4,800–7,070	1.1–1.7
LL1-alt[a]	6,830	170	6,820	6,520–7,130	1.1–1.7

*Leigh Lake earthquakes LL2–LL1 based on OxCal model 1. Superscript "a," an alternative time range for LL1 (LL1-alt) is based on OxCal model 2; however, we prefer the broader constraints of LL1 provided by model 1 (see the Geochronology section for discussion).

†Summary statistics in OxCal; earthquake probability density functions have 5 yr time bins.

‡Vertical displacement based on colluvial wedge thickness and total vertical separation across the central and eastern scarps (Fig. 3).

generated minor (centimeter-scale) distributed faulting. Earthquake LL1 occurred at ~5.9 ka (4.8–7.1 ka; 95%; preferred model), had a vertical displacement of ~1.1–1.7 m, and ruptured both the central and eastern scarps. LL1 is slightly older (~6.8 ka, 6.5–7.1 ka at 95%) in our alternative model; however, we prefer the younger (~5.9-ka) and broader constraint on LL1. ^{14}C and OSL ages from the unfaulted scarp-derived colluvial units in both trenches indicate that the central and eastern scarps have not ruptured since ~5 ka.

Completeness of the Paleoseismic record at the Leigh Lake Site

Our investigation at the Leigh Lake site likely documents a partial record of postglacial surface-faulting earthquakes on the central section of the Teton fault. Geomorphic mapping shows that Holocene surface faulting at Leigh Lake consists of distributed normal and oblique-slip faults within an ~1.5-kilometer-wide left step in the trace of the Teton fault (Figs. 2 and 3). South of Leigh Lake, the subparallel and east-facing western, central, and eastern scarps (Fig. 3) are formed on a deglacial surface within this stepover zone. We document evidence of LL2 (~10.0 ka) and LL1 (~5.9 ka) on the central and eastern scarps; however, the western scarp, which has 1.2–2.9 m of VS, remains unstudied. Thus, the total record of postglacial events on the western, central, and eastern scarps is likely incomplete.

The total VS across the western, central, and eastern scarps may also signal an incomplete postglacial earthquake record near Leigh Lake. The total VS across these scarps is ≤7.2 m, several meters less than an average VS of 11.1 m for similar deglacial surfaces at Granite Canyon, Taggart Lake, and Bradley Lake. It is possible that the ~3.9 m displacement deficit at Leigh Lake relates to unrecognized (submeter scale) distributed faulting with the left step, a continuation of oblique-slip and normal scarps west of the three subparallel scarps, off-fault deformation (e.g., surface warping), a reduction in postglacial cumulative slip at the fault step and/or variable displacement along strike. Regardless of the origin, it is possible that this displacement difference indicates the presence of at least one surface-faulting earthquake that postdates deglaciation of the region but is not expressed on the western, central, or eastern scarps.

Comparison with Previous Paleoseismic Data

The Leigh Lake earthquake history expands the Teton fault earthquake record into the early Holocene and supports the mid-Holocene timing of the most recent earthquake 22 km to the south at Granite Canyon (Byrd, 1995; Fig. 8). Earthquake LL2 at ~10.0 ka predates both the oldest event observed at the Granite Canyon site (~8 ka) and mid- to late Holocene liquefaction features interpreted from northern Jackson Lake (~3–5 ka). Earthquake LL1 at ~5.9 ka (4.8–7.1 ka; 95% confidence range) overlaps with the ~4.7–7.9 ka age range of the most recent earthquake at Granite Canyon (Byrd, 1995). However, because of the broad ~2–3 ka age uncertainties for LL1 and the Granite Canyon most recent earthquake, these events could represent different earthquakes. Both LL1 and the Granite Canyon most recent earthquake are significantly older than the Snake River delta subsidence event interpreted in northern Jackson Lake at ~1.6 ka. However, these events overlap with the older end of the ~3–5 ka age range for the paleoliquefaction features (Pierce *et al.*, 1998). Although we did not observe the oldest event from Granite Canyon (~8.1 ka) in Leigh Lake trenches A or B, we consider the Leigh Lake record to be incomplete because of the lack of paleoseismic data for the western scarp.

Teton Fault Earthquake History

Paleoseismic results for the Teton fault indicate that at least three earthquakes have ruptured the fault since deglaciation of the region at ~14–15 ka (Licciardi and Pierce, 2018; Pierce *et al.*, 2018). These earthquakes occurred ~10 (LL2), ~8 (Granite Canyon penultimate event), and ~5–7 ka (LL1 and Granite Canyon most recent event). However, considering the broad, ~2–3 ka uncertainties for LL1 and the Granite Canyon most recent event, it is possible that these events represent separate Teton fault earthquakes.

Rupture lengths for the three Teton fault earthquakes are broadly defined but useful for estimating prehistoric earthquake moment magnitudes (M_w). The ~10 ka earthquake likely spanned at least 22 km of the fault between the Granite Canyon and Leigh Lake sites (Fig. 1; all length measurements in this section are linear end to end). A length of ~47 km is possible if this earthquake ruptured both the central and southern fault sections. Evidence of this earthquake has not been identified north of Leigh Lake; however, we cannot rule out an entire ~70-kilometer-long rupture in this event. Using all-fault-type surface-rupture-length–magnitude empirical regressions (Wells and Coppersmith, 1994; Wesnousky, 2008), these length estimates yield M_w estimates of 6.6–6.7 (minimum), 7.0 (rupture of southern and central sections), and 7.2 (maximum). The ~8 ka earthquake has only been identified at Granite Canyon and thus its length is undefined. Using the rupture of the southern section (20 km) and the entire Teton fault (~70 km) as minimum and maximum bounds, the M_w range is 6.6–7.2. The youngest rupture at ~5–7 ka may have continued between Granite Canyon and Leigh Lake (~22 km), and possibly as far north as the Snake River delta paleoliquefaction site. If the youngest ruptures at these three sites are correlative, this earthquake may have a rupture length of at least 43 km, and possibly ~70 km based on the total Teton fault length. These estimates yield M_w estimates of at least 6.6–6.7, but more likely M_w 7.0–7.2 based on the similar, mid-Holocene timing of the youngest rupture along the fault. Additional paleoseismic data for the Teton fault would serve to better refine the timing, lateral extent, and magnitudes of these surface-faulting earthquakes.

Conclusions

Our Leigh Lake paleoseismic investigation yields Holocene earthquake timing and displacement data for the previously unstudied central section of the Teton fault. Two trenches across the central and eastern scarps at Leigh Lake yield evidence of two surface-faulting earthquakes. Earthquake LL2 occurred at ~10.0 ka (9.7–10.4 ka; 95%), expanding the Teton fault earthquake record into the early Holocene. Earthquake LL1 occurred at ~5.9 ka (4.8–7.1 ka; 95%; preferred model). Because of the structurally complex zone of surface faulting at Leigh Lake and the unstudied western scarp, the earthquake history at Leigh Lake is likely incomplete. Comparing our results to previous paleoseismic data from Granite Canyon (southern section) suggests that at least three surface-faulting earthquakes ruptured the Teton fault at ~10, ~8, and ~5–7 ka. Rupture lengths and magnitudes remain poorly defined but are likely >20–22 km (M_w > 6.6–6.7) for the early Holocene events and >43 km (M_w > 7.0) for the 5–7-ka earthquake. Additional paleoseismic data for the Teton fault are required to more robustly constrain potential earthquake correlations and along-strike rupture lengths. Our data expand the early Holocene earthquake history of the Teton fault, confirm a late Holocene period of quiescence on the central and southern sections of the fault, and will inform future seismic hazard assessments of the region.

Data and Resources

Light detection and ranging (lidar) data used in this study and shown in Figures 2 and 3 were collected in 2014 by Grand Teton National Park (GRTE). The 1 m lidar data were provided by the National Park Service (NPS) office in Moose, Wyoming. Unit boundaries for federal land and parks shown in Figure 1 are from the NPS and downloaded from https://www.data.gov (last accessed July 2018). Streams and rivers shown in Figure 1 are from the U.S. Geological Survey Water Science Center's Watershed Boundary Dataset for Jackson County and Teton County, Wyoming, and were downloaded from http://datagateway.nrcs.usda.gov (last accessed January 2018). The digital elevation model base map for Figure 1 is ⅓-arcsec (10 m) resolution data from the U.S. Geological Survey National Elevation Dataset (NED). Data can be accessed at https://viewer.nationalmap.gov/basic/ (last accessed October 2019). All other data and resources used in this study are listed and cited in the article. The Ⓔ supplemental material includes additional photographs of the Leigh Lake site, trench wall photomosaics, stratigraphic unit descriptions, scarp profiles and vertical-separation measurements, and the OxCal Bayesian modeling software (v.4.3) code used in this study.

Acknowledgments

This research was funded by the University of Wyoming and National Park Service Research Station small grants program, Idaho State University (ISU), U.S. Geological Survey (USGS), and BGC Engineering, Inc. National Science Foundation Grant EAR 1755079 to ISU also supported the latter stages of the research. Nick Patton, Carl Jurkowski, and Alison Trcka of ISU and Darren Zellman assisted with many aspects of the fieldwork. The authors thank Grand Teton National Park for interest in this research and for assisting with permitting and site access. The authors also thank *BSSA* reviewers Katherine Scharer and Christoph Grützner, and USGS reviewer Ryan Gold (USGS) for constructive comments that improved this article. An anonymous *BSSA* reviewer provided helpful comments on the Ⓔ supplemental content. Any use of trade, firm, or product names is for descriptive purposes only and does not imply endorsement by the U.S. Government.

References

Bronk Ramsey, C. (2009). Bayesian analysis of radiocarbon dates, *Radiocarbon* **51,** no. 1, 337–360.

Byrd, J. O. D. (1995). *Neotectonics of the Teton fault, Wyoming*, *Doctoral Dissertation*, University of Utah, Salt Lake City, Utah.

Byrd, J. O. D., R. B. Smith, and J. W. Geissman (1994). The Teton fault, Wyoming: Topographic signature, neotectonics, and mechanism of deformation, *J. Geophys. Res.* **99,** no. B10, 20,095–20,122.

DuRoss, C. B., S. E. K. Bennett, R. W. Briggs, S. F. Personius, R. D. Gold, N. G. Reitman, A. I. Hiscock, and S. A. Mahan (2018). Combining conflicting Bayesian models to develop paleoseismic records: An example from the Wasatch fault zone, Utah, *Bull. Seismol. Soc. Am.* **108,** 3180–3201, doi: 10.1785/0120170302.

DuRoss, C. B., M. P. Bunds, R. D. Gold, R. W. Briggs, N. G. Reitman, S. F. Personius, and N. A. Toké (2019). Variable normal-fault rupture behavior, northern Lost River fault zone, Idaho, USA, *Geosphere* doi: 10.1130/GES02096.1 (in press).

DuRoss, C. B., R. D. Gold, R. W. Briggs, J. E. Delano, D. A. Ostenaa, M. Zellman, N. Cholewinski, S. Wittke, and S. A. Mahan (2019). Holocene earthquake history and slip rate of the southern Teton fault, Wyoming, USA, *Geol. Soc. Am. Bull.* doi: 10.1130/B35363.1.

Gilbert, J. D., D. A. Ostenaa, and C. Wood (1983). Seismotectonic study Jackson Lake Dam and Reservoir, Minidoka Project, Idaho-Wyoming: Denver, Colo., U.S. Department of the Interior, *U.S. Bureau of Reclamation Seismotectonic Report 83-8*, 123 pp.

Gray, H. J., S. A. Mahan, T. Rittenour, and M. Nelson (2015). Guide to luminescence dating techniques and their applications for paleoseismic research, in W. R. Lund (Editor), *Proc. Volume, Basin and Range Province Seismic Hazards Summit III (BRPSHSIII)*, Utah Geol. Surv. Misc. Pub. 15-5, variously paginated.

Hampel, A., R. Hetzel, and A. Densmore (2007). Postglacial slip-rate increase on the Teton normal fault, northern Basin and Range Province, caused by melting of the Yellowstone ice cap and deglaciation of the Teton Range? *Geology* **35,** no. 12, 1107.

Licciardi, J. M., and K. L. Pierce (2018). History and dynamics of Greater Yellowstone Glacial System during the last two glaciations, *Quaternary Sci. Rev.* **200,** 1–33.

O'Connell, D. R. H., C. K. Wood, D. A. Ostenaa, L. V. Block, and R. C. LaForge (2003). Ground motion evaluation for Jackson Lake Dam, Minidoka project, Wyoming: Denver, Colorado, *Bureau of Reclamation Report 2003-2*, 493 pp.

Petersen, M. D., M. P. Moschetti, P. M. Powers, C. S. Mueller, K. M. Haller, A. D. Frankel, Y. Zeng, S. Rezaeian, S. C. Harmsen, O. S. Boyd, *et al.* (2014). Documentation for the 2014 update of the United States national seismic hazard maps, *U.S. Geol. Surv. Open-File Rept. 2014-1091*, 243 pp.

Pierce, K. L., and J. D. Good (1992). Field guide to the Quaternary geology of Jackson Hole, Wyoming, *U.S. Geol. Surv. Open-File Rept. 92-504*, 54 pp.

Pierce, K. L., J. M. Licciardi, J. M. Good, and C. Jaworowski (2018). Pleistocene glaciation of the Jackson Hole area, Wyoming, *U.S. Geol. Surv. Profess. Pap. 1835*, 56 pp., doi: 10.3133/pp1835.

Pierce, K. L., S. Lundstrom, and J. M. Good (1998). Geologic setting of archaeological sites in the Jackson Lake area, Wyoming, in *Final Report on the Jackson Lake Archaeological Project, Grand Teton National Park, Wyoming*, M. A. Connor (Editor), Report prepared for Bureau of Reclamation, Pacific Northwest Office, Boise, ID, Technical Report No. 46, Department of the Interior, National Park Service, Midwest Archeological Center, Lincoln, Nebraska, 278 pp.

Prescott, J. R., and J. T. Hutton (1994). Cosmic ray contributions to dose-rates for luminescence and ESR dating: Large depths and long-term time variations, *Radiat. Meas.* **23,** 497–500.

Puskas, C. M., R. B. Smith, C. M. Meertens, and W. L. Chang (2007). Crustal deformation of the Yellowstone–Snake River Plain volcano-tectonic system: Campaign and continuous GPS observations, 1987–2004, *J. Geophys. Res.* **112,** no. B03401, doi: 10.1029/2006JB004325.

Reitman, N. G., S. E. K. Bennett, R. D. Gold, R. W. Briggs, and C. B. DuRoss (2015). High resolution trench photomosaics with structure from motion: Workflow and accuracy assessment, *Bull. Seismol. Soc. Am.* **105,** no. 5, 2354–2366, doi: 10.1785/0120150041.

Rhodes, E. J. (2011). Optically stimulated luminescence dating of sediments over the past 200,000 years, *Ann. Rev. Earth Planet. Sci.* **39,** 461–488, doi: 10.1146/annurev-earth-040610-133425.

Smith, R. B., J. O. D. Byrd, and D. D. Susong (1993). *The Teton Fault, Wyoming—Seismotectonics, Quaternary History, and Earthquake Hazards*, in Geology of Wyoming, Geological Survey of Wyoming Memoir No. 5, Snoke, J. R. Steidtmann, and S. M. Roberts (Editors), 628–667.

Thackray, G. D., and A. E. Staley (2017). Systematic variation of late Pleistocene fault scarp height in the Teton Range, Wyoming, USA: Variable fault slip rates or variable landform ages? *Geosphere* **13,** no. 2, 287–300, doi: 10.1130/GES01320.1.

Thackray, G. D., C. B. DuRoss, M. S. Zellman, S. Wittke, R. D. Gold, J. Delano, J. A. T. Jobe, M. Hille, K. Grasso, and S. Mahan (2019). Is the Antelope Flats fault an antithetic rupture of the Teton fault? *Seismol. Res. Lett.* **90,** no. 2b, 901–902.

Wells, D. L., and K. J. Coppersmith (1994). New empirical relationships among magnitude, rupture length, rupture width, rupture area and surface displacement, *Bull. Seismol. Soc. Am.* **84,** 974–1002.

Wesnousky, S. G. (2008). Displacement and geometrical characteristics of earthquake surface ruptures: Issues and implications for seismic-hazard analysis and the process of earthquake rupture, *Bull. Seismol. Soc. Am.* **98,** 1609–1632, doi: 10.1785/0120070111.

White, B. J. P., R. B. Smith, S. Husen, J. M. Farrell, and I. Wong (2009). Seismicity and earthquake hazard analysis of the Teton-Yellowstone region, Wyoming, *J. Volcanol. Geoth. Res.* **188,** nos. 1/3, 277–296.

Zellman, M. S., C. B. DuRoss, and G. D. Thackray (2019). The Teton fault, *Wyoming Geological Survey Open-File Rept. 2019-1*, scale 1:75,000.

Mark S. Zellman
BGC Engineering, Inc.
701, 12th Street, Suite 211
Golden, Colorado 80401 U.S.A.
mzellman@bgcengineering.com

Christopher B. DuRoss
Stephen F. Personius
U.S. Geological Survey
MS 966
P.O. Box 25046
Denver, Colorado 80225 U.S.A.

Glenn D. Thackray
Department of Geosciences
Idaho State University
921 South 8th Avenue
Box 8072
Pocatello, Idaho 83209 U.S.A.

Nadine G. Reitman
Department of Geological Sciences
University of Colorado Boulder
2200 Colorado Avenue, UCB 399
Boulder, Colorado 80309 U.S.A.

Shannon A. Mahan
U.S. Geological Survey
MS 974
P.O. Box 25046
Denver Federal Center
Denver, Colorado 80225 U.S.A.

Cooper C. Brossy
P.O. Box 424
Shoshone, Idaho 83352 U.S.A.

Manuscript received 22 May 2019